Human graft cornea and laser incisions imaging with micrometer scale resolution full-field optical coherence tomography

Gaël Latour
Gaëlle Georges
Laure Siozade Lamoine
Carole Deumié
Aix-Marseille Université
Ecole Centrale Marseille
CNRS
Institut Fresnel
Domaine Universitaire de Saint-Jérôme
13397 Marseille Cedex 20, France

John Conrath
Louis Hoffart
Aix-Marseille Université
Hôpital de la Timone
Service d'Ophtalmologie
264 rue Saint Pierre
13385 Marseille Cedex 5, France

Abstract. Micrometer scale resolution full-field optical coherence tomography (FF-OCT) is developed for imaging human graft corneas. Three-dimensional (3-D) images with ultrahigh resolution (respectively, 1 and 1.5 μm in the axial and transverse directions), comparable to traditional histological sections, are obtained allowing the visualization of the cells and the precise structure of the different layers that compose the tissue. The sensitivity of our device enables imaging the entire thickness of the cornea, even in edematous corneas more than 800 μm thick. Furthermore, we provide tomographic 3-D images of laser incisions inside the tissue at various depths without slicing the studied corneas. The effects of laser ablations can be observed, along various optical sections, directly in the bulk of the sample with high accuracy, providing information on the interface quality and also imaging tiny changes of the tissue structure. FF-OCT appears to be a powerful tool for subcellular imaging of the corneal structure and pathologies on the entire thickness of the tissue as well as interface quality and changes in the collagen structure due to laser incisions on *ex vivo* human cornea. [DOI: 10.1117/1.3486544]

Keywords: optical coherence tomography; ultrahigh resolution imaging; ophthalmology; cornea; laser surgery.

Paper 10109RRR received Mar. 4, 2010; revised manuscript received Jun. 25, 2010; accepted for publication Jul. 26, 2010; published online Sep. 17, 2010.

1 Introduction

Noninvasive techniques are of particular relevance in ophthalmology. Optical techniques are attractive because they often enable *in vivo* and *in situ* diagnosis. More generally, imaging techniques can provide key information about the structure and early detection of diseases without tissue preparation or slicing because they provide virtual biopsies from the tissues inside an acquired volume of data. Different slices can be realized inside the observed volume, along planes parallel to the surface, as is usually the case in optical microscopy, or along axial planes, so that images can be compared to histological sections of the tissues.

Confocal reflectance microscopy selects light scattered for a given depth using spatial filtering to reject the light scattered by the rest of the sample. It is currently used for *in vivo* cornea imaging at the cell-scale level.[1–4] Multiphoton microscopy provides very informative images of the cornea.[5–10] This technique is based on the nonlinear excitation of fluorescent molecules or on harmonic generation. The excitation occurs only in a confined focal volume and, using high-numerical-aperture objectives, subcellular information can be achieved. Different nonlinear effects produce different wavelengths, enabling multimodal imaging of the same sample, highlighting several structures: two-photon excited fluorescence (2PEF) (epithelial and endothelial cells, stromal keratocytes), second-harmonic generation (SHG) (collagen lamellae in the stroma), and third-harmonic generation (THG) (epithelial and endothelial cells, stromal keratocytes). Optical coherence tomography (OCT) has also emerged as a new technology for 3-D imaging.[11,12] Its high axial resolution, good penetration depth, high sensitivity, noninvasive and nondestructive nature, and the possibility of real-time imaging make OCT interesting for a wide range of biomedical applications. OCT is particularly suitable for ophthalmology because of the transparency of the eye. OCT performs imaging along a great depth of both the anterior segment and the retina.

OCT is based on the principle of interferometry using a low-temporal-coherence source. A light source with a wide spectrum is used to achieve high axial resolution, around a micrometer for state-of-the-art devices. Fourier-domain OCT (FD-OCT) is widely used in ophthalmology as a high-speed method for *in vivo* imaging of the retina[13,14] but also of the anterior segment of the human eye.[15,16] Nevertheless, this technique, based on the Fourier transform of the signal coming from the entire depth of the sample, is based on the use of a low-numerical-aperture objective that limits the transverse resolution to reach great depths of field. It then implies a

Address all correspondence to: Laure Siozade-Lamoine, Domaine Universitaire de Saint-Jérôme, Institut Fresnel, CNRS, Aix-Marseille Université, Ecole Centrale Marseille, 13397, Marseille Cedex 20, France, Tel: 33-49-1288-393. E-mail: laure.siozade@fresnel.fr

1083-3668/2010/15(5)/056006/9/$25.00 © 2010 SPIE

compromise between the desired transverse resolution and the axial extent of the images. This type of FD-OCT presents complex optical design and is quite expensive. For certain applications, such as high-resolution imaging of the cornea cells along the entire thickness of the tissue, full-field OCT (FF-OCT) is an attractive alternative.[17] A two-dimensional (2-D) image is recorded at a selected depth and the axial shift of the sample enables recording the information as a function of the third dimension. The setup is based on a Michelson interferometer including two identical microscope objectives. In our case, the light source is a halogen lamp that presents a broad and smooth spectrum, achieving imaging with high axial resolution. This configuration provides the possibility of using high-numerical-aperture objectives for increasing the transverse resolution. FF-OCT reaches micrometer-scale imaging[18,19] and has already demonstrated its potential for imaging porcine and mouse eyes[20] but also human donor cornea[21] with a spatial resolution of $2.0 \times 2.4\ \mu m^2$.

Laser surgery is currently a "gold standard" in ocular surgery. Femtosecond lasers are routinely used for the laser *in situ* keratomileusis (LASIK) procedure, which is a refractive surgical technique for the correction of ocular optic errors.[22–26] The femtosecond laser provides a precise and safe dissection for the realization of the corneal flap.[27] More recently, this laser was also used for keratoplasty.[28,29] In this case, a custom-shaped grafting of the tissue is performed related to the pathology. The size and the shape of the donor and recipient cuts are determinant criteria in obtaining an accurate fit and good visual outcomes. The great advantage of the laser procedure over the mechanical techniques is the 3-D abilities of the laser dissection of the tissue, enabling several keratoplasty techniques. Various shapes can be realized and the laser incisions can be adapted to the precise location of the need of the graft.[30] This surgical device appears as very safe and predictable because of the good reproducibility of laser incisions.[31] Nevertheless, most of the studies detail the interaction process between the short pulses of the laser and the corneal tissue to determine the threshold irradiance.[32] The shape and the precise size of the disrupted tissue is mainly studied on histological sections by optical and electron transmission microscopy.[33,34] It has been proven that OCT imaging can perform interesting information for glaucoma surgery[35] or for corneal surgery[36] but with a few micrometers resolution. The use of an imaging technique, that provides a 1×1.5-μm resolution, to improve the laser surgery and to achieve a better cut of the cornea for corneal graft is of great interest for the surgeon, providing information on the interface quality and also imaging tiny changes of the tissue structure and the presence of small cavitation bubbles.

In this paper, we describe FF-OCT, providing micrometer-scale resolution imaging of human graft corneas. First, the optical device, adapted to the study of immerged corneas, is presented and characterized. Imaging of human donor corneas is then realized, showing the possibility of visualizing the fine structures of the tissue on the entire thickness. The particular cases of edematous corneas and of laser incisions inside graft corneas are detailed. The interest of FF-OCT is that the data volume can be observed directly with a high resolution, close to histological section views, and according to different optical slices. It then appears as a powerful tool for the study of *ex vivo* human cornea and for the improvement of the laser incisions.

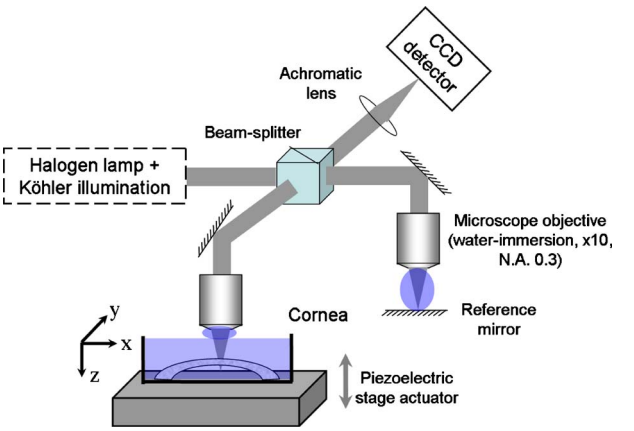

Fig. 1 Schematic representation of the full-field OCT setup with an immerged cornea as the probed sample.

2 Experimental Setup and Methods

2.1 *Full-Field OCT Setup*

OCT is an optical technique using the principle of white light interferometry.[11] The setup is based on a Michelson interferometer utilizing a broadband light source where one mirror is replaced by the studied sample.[17] Interference patterns are visible only if the optical path difference between both arms is smaller than the coherence length of the source. Low coherence length results in interference patterns with a restricted axial extension and consequently a precise location of the sample interfaces. Moreover, the use of a microscope objective performs an increase of the lateral resolution as in optical microscopy. In our case, two identical microscope objectives are included in each arm to obtain interference patterns when the beams are recombined, leading to a Linnik interferometer microscope.[18] Water immersion objectives are chosen to reduce the light reflection from the surface of the sample and to avoid dispersion mismatch between both arms,[19] especially in the case of an immerged sample.

Our experimental implementation is a full-field time domain OCT device (see Fig. 1). The light source is a halogen lamp coupled with a Köhler illumination for a homogeneous illumination. The incident light is split into two arms by a beamsplitter cube with a working range between 700 and 1100 nm. In both arms, mirrors oriented at a 45-deg angle reflect light vertically to use immersion objectives with horizontal samples. Two identical water-immersion microscope objectives [$\times 10$, 0.3 numerical aperture (NA), Olympus] are used to provide good transverse resolution. A glass slab is placed in the reference arm and serves as a fixed reference mirror. The sample is mounted on a high-precision linear stage (M-714, Physik Instrument PI), which provides a maximum displacement of 7 mm. This shift is obviously much longer than the penetration depth because of the absorption and the scattering properties of the sample. After recombination, both beams are focused with a 30-mm achromatic lens on the detector. The frames are recorded by a CCD camera, sensitive from 400 to 1000 nm, composed of a

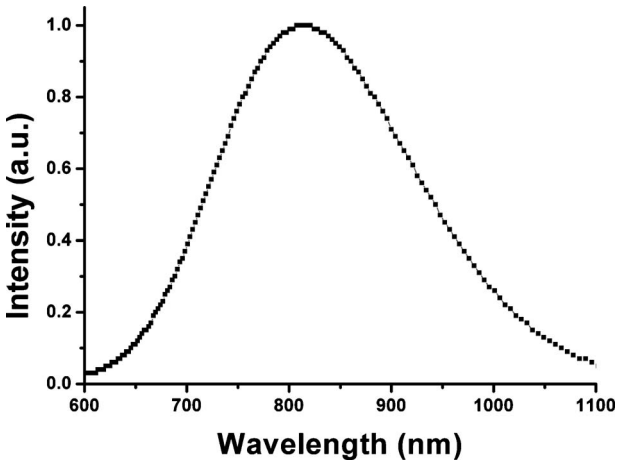

Fig. 2 Spectral sensitivity of the FF-OCT setup

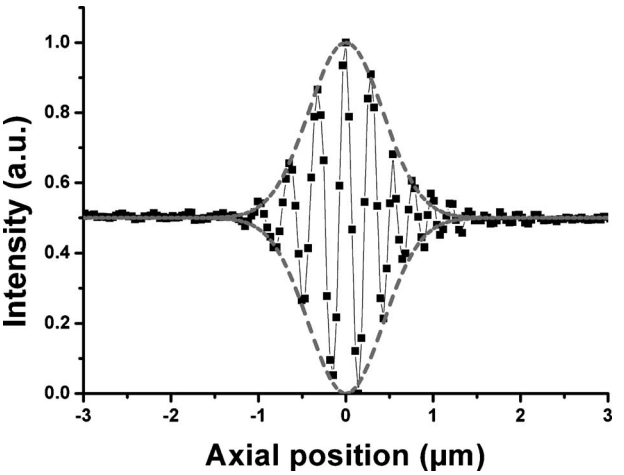

Fig. 3 Interferogram obtained from a glass slab (dotted line); each point corresponds to the recorded intensity as a function of the axial shift of the sample and the Gaussian shape modeled envelops (dashed line) with a FWHM equal to 1 μm which gives the experimental axial resolution.

659-×494-pixel matrix and that can reach 200 frames/s (GC 660, Prosilica). To increase the sensitivity of the device, 2-×2-pixel binning is performed, reducing the number of effective pixels to 329×247.

2.2 *Image Acquisition and System Characteristics*

2.2.1 *Principle of the image acquisition*

The CCD camera and the piezoelectric stage are driven by a computer interface. The experimental device enables the acquisition of optical slices at different depths. The recorded information is composed of the incoherent light coming from both arms and of the superimposed fringe patterns. For each position, at a fixed depth inside the sample, the measurement consists of the subtraction in two frames with a phase shift equal to π that corresponds to a shift of the sample equal to 150 nm in water.[37,38] We record this calculated frame, which gives access to the fringe envelope and can be considered as an optical slice at the studied depth. Furthermore, at each position, a number of N frames is averaged for a better imaging sensitivity. Since the refractive index of the cornea ($\sim$1.37) is quite close to the one of the water (1.33), the optical thickness measured by OCT is quite the same as the physical thickness. All the axial distances indicated in the figures are optical thicknesses.

2.2.2 *Spectral sensitivity*

The spectral transfer function of the setup was optimized for the study of biological samples, that is, in the near-IR range. Experimentally, this function mainly depends on both the camera spectral sensitivity and the emission spectrum of the light source. The halogen lamp is a thermal light source and its spectrum is centered in the IR spectral range and reaches the lowest wavelengths of the visible range when the intensity is high enough. The effective spectral sensitivity is the multiplication of both spectra and is limited by the halogen lamp at the lowest wavelengths and by the camera at the highest ones. The experimental spectral transfer function of our optical setup is calculated from the Fourier transform of the interferograms recorded on a glass sample, assuming that the Fresnel reflection coefficient of this material is independent of the wavelength (see Fig. 2). In our case, the spectral transfer function is centered at 810 nm and exhibits a 230-nm full width at half maximum (FWHM). All the optical elements (beamsplitter, mirrors, microscope objectives, achromatic lens) used in the setup were chosen for their optimal optical properties in this spectral range.

2.2.3 *Axial and transverse resolutions*

The axial resolution Δz (i.e., in the z direction in the Fig. 1) depends on the source coherence length l_c. Interference fringes are visible only if the optical path difference between both arms is smaller than the temporal coherence length of the source. The axial resolution is generally defined as the FWHM of the interferogram. If the source is assumed to have a Gaussian spectrum, the axial resolution, which depends on the mean wavelength λ_0, on the FWHM $\Delta\lambda$ of the effective spectrum and on the refractive index of the medium n, can be written as

$$\Delta z = \frac{l_c}{2} = \frac{2\ln 2}{n\pi}\frac{\lambda_0^2}{\Delta\lambda}.$$

In our case, the experimental axial resolution in water was measured to be 1 μm for a 0.95-μm theoretical one (see Fig. 3). Note that this axial resolution is degraded at depths of several hundred micrometers due to dispersion mismatch in the two interferometer arms relative to the studied tissue in the sample arm.[19]

The transverse resolution (i.e., in the x and y directions in Fig. 1) is limited by the diffraction. The Rayleigh criterion was used to determine the minimum resolvable detail. The theoretical resolution r is then given by the numerical aperture of the objectives NA and the center wavelength of the effective spectrum λ_0:

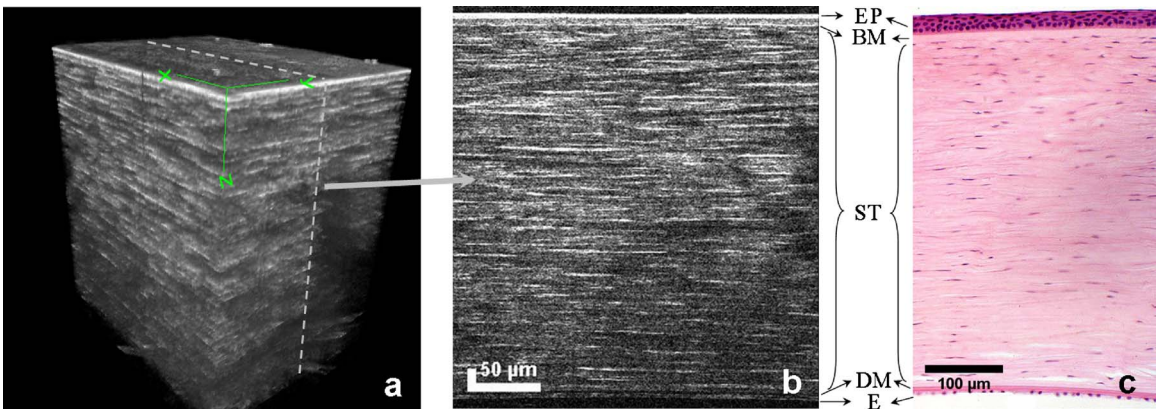

Fig. 4 (a) Three-dimensional tomographic image of the entire thickness of the cornea ($250 \times 190 \times 900$ μm^3 stack, with 1-μm axial steps) and (b) for a better view of the cornea structure a cross section of the 3-D OCT image is shown (along the dashed line). The different structures that comprised the cornea are indicated: epithelium (EP), Bowman's membrane (BM), stroma (ST), Descemet's membrane (DM), and endothelium (E), and (c) can be compared to a histological section of a healthy cornea.

$$r = \frac{\lambda_0}{2\mathrm{NA}}.$$

In our case, the theoretical transverse resolution is 1.4 μm and it was experimentally measured to be 1.5 μm. The resolution is degraded when imaging is performed through biological tissues with complex features that induce a distortion of the optical wavefront and multiple scattering effects. The field of view of the camera is a 250- $\times$ 190-μm^2 rectangle. To conclude, our experimental device enables 3-D imaging with a micrometer scale in the three directions.

2.2.4 *Detection sensitivity*

The maximum penetration depth that can be reached by OCT is defined by the ability of the device to detect the signal backscattered at this depth. The detection sensitivity depends on the SNR, which could be increased by the average of N images for a fixed position. By considering that the detection system is shot-noise limited and that the CCD camera operates close to saturation,[19] the experimental detection sensitivity is about 93 dB for an average of 200 frames. It corresponds to a trade-off between the detection sensitivity and the acquisition time (around 7 ms per frame, which means that is around 3 s for a tomographic image).

2.3 *Human Cornea and Laser Surgery*

Human corneoscleral rims were obtained from the eye bank (French Blood Center, Marseille, France). This study is based on a corpus of 10 human donor corneas to ensure representative results. All specimens were tissues rejected for transplantation based on standard operating protocols specified by the European Eye Bank Association, mainly due to their low endothelial cell density (below 2000 cells/mm^2), but these corneal grafts remain representative for the study of the cornea structure, especially for the stroma structure. The eyes were obtained within 36 h after death and stored in Optisol-GS. The storage in Optisol-GS does not exceed 10 days. Corneas were delivered in CorneaMax (Eurobio, Les Ulys, France) medium. Some corneas were directly imaged, intact, immerged in balanced salt solution (BSS). The other corneas were used to study laser surgery effects in the corneal tissue. After completion of the cut, the corneal button was replaced in CorneaMax and OCT imaging was performed within 48 h.

Corneal incisions were performed using a Femtec laser (Tecnolas PerfectVision©, Heidelberg, Germany). This apparatus consists of a pulsed solid-body (Nd:glass) laser with a repetition rate of 40 kHz that emits light with a wavelength of 1055 nm and a pulse duration of 500 to 800 fs. Laser beam energy of 3.2 to 3.4 μJ and a spot separation of 3 μm were chosen. To cut the corneal specimen, corneoscleral discs were inserted in an artificial anterior chamber (Moria, Antony, France). Sodium hyaluronate 1.4% (Healon, AMO, Ettlingen, Germany) was instilled in the artificial anterior chamber as a viscoelastic up to a pressure of 20 mm Hg. Then, the corneas were mounted on the Femtec laser through an aplanation lens and centered using the reflex image of the diode lights of the laser. The aplanation lens provided by Tecnolas Perfect Vision is curved with a 10.5-mm radius of curvature. The cutting process was performed from posterior to anterior (i.e., a circular movement of the laser beam was used to cut through endothelium, stroma forward to the corneal epithelium). Patterns of the corneal incisions were as follows. First, the laser was set to obtain a deep lamellar corneal cut (parallel to the corneal surface) set at 160 μm deep, then corneal vertical cuts were performed, i.e., the angle for the cut edge was set at 90 deg to achieve a cut line running perpendicular to the surface tangent. The cornea was then disconnected from the laser and the corneal button was replaced in CorneaMax for further examination. After removal of the sample from the initial solution and during the preparation of the tissue, the hydration of the corneal surface was maintained by instillation of BSS. Nevertheless, BSS on the surface is not used during laser experiments to avoid any excess of liquid that could interfere with the measurements. The sample preparation did not exceed 10 min. Afterward, it is crucial to minimize the experiment duration, to limit the dehydration of the corneal samples.

3 Human Graft Cornea Imaging

3.1 *Human Graft Corneas*

Figure 4(a) shows a 3-D tomographic image of the entire

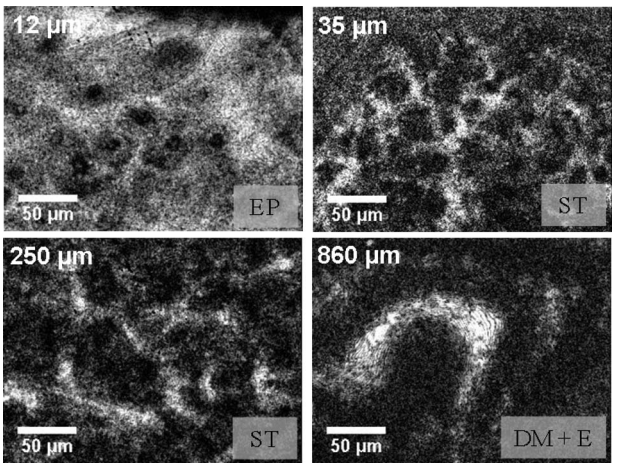

Video 1 Two-dimensonal tomographic images along the transverse planes from the previous stack shown in Fig. 4 ($250\times190\times900$ μm^3 stack, with 1-μm axial steps); the scale bar is 50 μm and the depth is indicated in the upper left corner. The different structures that comprised the cornea are visible: epithelium (EP), Bowman's membrane (BM), stroma (ST), Descemet's membrane (DM), and endothelium (E). At 35 and 250 μm deep in the corneal stroma, the keratocytes are identified with their specific shape (QuickTime, 4.4 MB). [URL: http://dx.doi.org/10.1117/1.3486544.1].

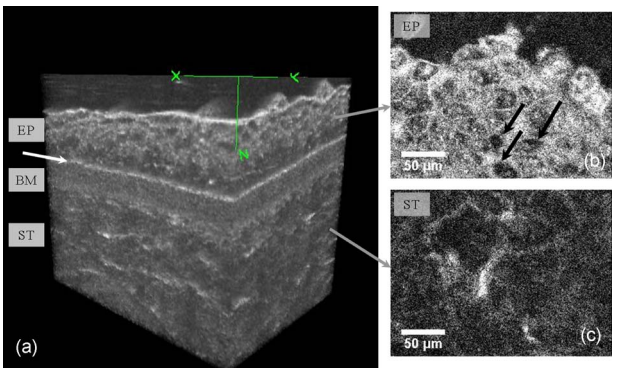

Fig. 5 (a) Three-dimensional tomographic image of the surface of the cornea ($250\times190\times150$ μm^3 stack, with 0.5-μm axial steps) with the epithelium (EP), the Bowman's membrane (BM), the basement membrane (white arrow) and the anterior stroma (ST), and (b) and (c) 2-D tomographic images along the transverse direction respectively in the epithelium with the hyporeflective corneal epithelial bullae (black arrows) and in the stroma.

thickness of the cornea with 1-μm scanning steps. One of the axial cross sections of the previous volume of data is presented in Fig. 4(b). We can see that the epithelium (EP), Bowman's layer (BM), stroma (ST), Descemet's membrane (DM), and endothelium (E) from the anterior surface to the posterior surface of the cornea are clearly differentiated. These different layers can be easily identified as on routine histological corneal tissue sections [see Fig. 4(c)]. The recorded signal level is quite high also from the deeper areas, and the posterior interface can be precisely located even if the light crosses 800 μm of corneal tissue. Furthermore, imaging quality is good despite this relatively great depth. This is mainly due to the weak dispersion mismatch in the two interferometer arms and to the transparency property of the cornea.

Figure 4(b) shows a stacked organization with bright interfaces parallel to the surface of the cornea. This light reflection is due to the keratocytes in the corneal stroma. These cells are parallel to each other and the collagen lamellae are located between them. The stacked organization of the collagen lamellae can be identified on the axial tomographic image, because they appear between the keratocytes with a lower signal. In the posterior part, most of the collagen lamellae tended to be arranged parallel to the corneal surface. The organization revealed by the OCT appears remarkably similar to that of the histological section.

From the same 3-D tomographic data, cross sections parallel to the surface of the cornea can be realized (see Video 1). At around 10 μm deep, inside the epithelium, the epithelial cells and the nuclei boundaries are clearly visible on the transverse slices. Highly scattering structural details revealing the uppermost stromal keratocytes are visible at around 35 μm deep, just above the basement membrane. In this example, the low thickness of the epithelium is related to the manipulation for tissue preparation at the Eye Bank and before OCT imaging. The keratocytes are imaged along the entire thickness of the cornea and their number decreases from the anterior to the posterior stroma. Finally, the endothelial layer appears at around 800 μm deep. At this level, we can observe folds in Descemet's membrane, observed as an arched structure. Hexagonal structures imaged at the level of endothelium correspond to endothelial cells.

At approximately 300 μm below Bowman's layer (tomographic image in the lower left corner of Video 1), the keratocyte network is revealed as flat cells connected by cytoplasmic processes, linking adjacent cells together. Keratocytes give a high tomographic signal, even in a deep region of the stroma, and they can easily be recognized along the entire thickness of the cornea. Axial tomographic views [Fig. 4(b)] are projections of the transverse views. The characteristic stacked organization is due to the tomographic signal of the keratocytes projected on a perpendicular plane.

In Fig. 5, only the first 125 μm of the corneal structure are shown with an axial acquisition step reduced to 0.5 μm for a better imaging quality in the axial direction. The dynamic views of these tomographic data are presented on Video 2. Intraepithelial layers [EP layer in Fig. 5(a) transverse view is presented in Fig. 5(b)], Bowman's layer [BM in Fig. 5(a)], and anterior stroma [ST in Fig. 5(a)] are clearly visualized from the anterior to the posterior part of the cornea. The resolution of the system is high enough to distinguish even intraepithelial layers and some epithelial wing cells appear at the top of the 3-D image. The transverse sections of the epithelium [Fig. 5(b)] show the nucleis of the epithelial cells. The high-resolution images show a thickened epithelium with hyporeflective corneal epithelial bullae [black arrows in Fig. 5(b)], corresponding to intraepithelial edema vacuoles. The position of the Bowman's membrane can be clearly located [BM in Fig 5(a)]. This membrane appears as a dark band with a thickness of 20 μm. The thin and curved layer oriented parallel to the corneal surface just above Bowman's layer [see white arrow in Fig. 5(a)] can be identified as the basement membrane. In Fig. 5(c), we could observe the anterior stroma. In this layer, the specific shape of the keratocytes is seen as a bright pattern surrounded by scattering collagen fibrils.

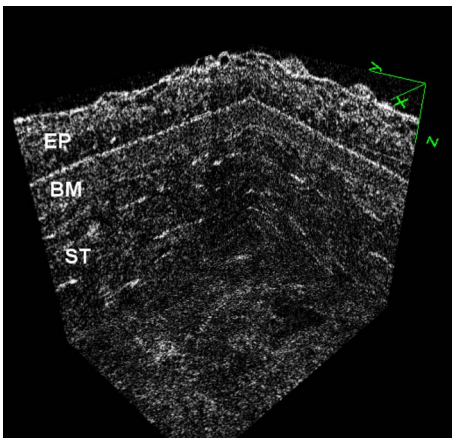

Video 2 Two-dimensional tomographic dynamic views of the upper part of the cornea ($250\times190\times150$ μm^3 stack, with 0.5-μm axial steps) along the different planes, successively transverse and axial. The epithelium (EP), the Bowman's membrane (BM), and the anterior stroma (ST) are visible on these different views (QuickTime, 3.6 MB). [URL: http://dx.doi.org/10.1117/1.3486544.2].

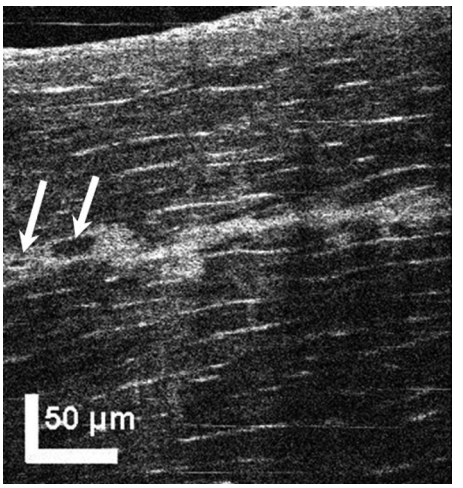

Video 3 Two-dimensional tomographic images along the axial direction; arrows indicate the microcavities due to the laser incisions at 160 μm deep in the stroma 36 h after laser surgery; scale bar is 50 μm ($250\times190\times350$ μm^3 stack, with 0.5-μm axial steps) (QuickTime, 1.1 MB). [URL: http://dx.doi.org/10.1117/1.3486544.3].

3.2 *Edematous Corneas*

OCT imaging was also performed on edematous corneas (see Fig. 6) and enabled the observation of the water accumulation regions that are formed between stromal lamellae in strongly edematous corneas. The presence of water in the stroma appears as dark regions on the images because there is no light scattering in these regions and, hence, no tomographic signal is recorded. In these pathologic conditions, the degree of organization of the collagen fibers is decreased and the amount of interstitial fluid is increased. Large fluid vacuoles are present between lamellae, the so-called "lakes,"[39] resulting in distortion of fibrillar collagen distribution. On nonedematous cornea grafts, keratocytes are the main cells observed in the stroma with OCT imaging, whereas on an edematous cornea stromal lamellae become clearly visible [see Figs. 6(b) and 6(c)], mainly due to the refraction index mismatch between the lakes, composed of water, and the collagen lamellae.

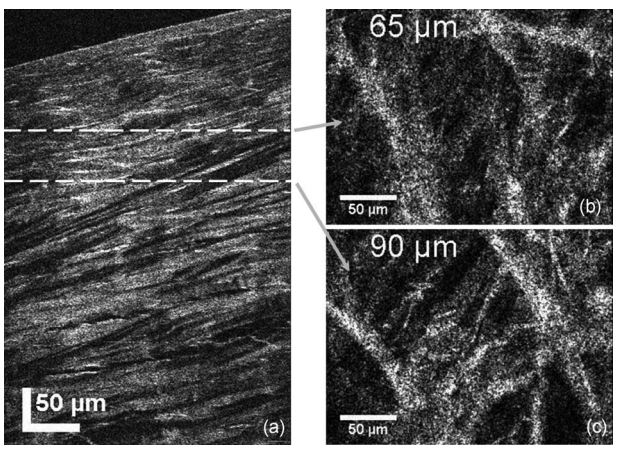

Fig. 6 Tomographic images ($250\times190\times450$ μm^3 stack, with 0.5-μm axial steps) along (a) the axial and (b) and (c) the transverse directions at 65 and 90 μm deep of an edematous cornea.

In parallel to these physiological changes, it is well known that the swelling of the cornea is correlated with a clinical reduction of the transparency of the tissue and a modification of its optical properties.[40,41] The observation of the growth of such edema is then very interesting for a good understanding of these mechanisms.

3.3 *Laser Surgery*

The effect of femtosecond laser incisions in clear corneal tissue, at threshold exposure and above, can also be observed by ultrahigh-resolution OCT. Lamellar incisions were performed in the anterior stroma of human cornea at 160 μm deep (see Video 3). In this geometry, laser cuts are parallel to the corneal surface and show a slightly irregular cut pattern. The cutting edge inside the stroma is easily visible. The perturbation of the collagen structure extends to only a few micrometers of depth in the tissue and a hyperdensification of the collagen is visible at the borders of the incision, corresponding to disordering and delamination effects. Normal adjacent collagen fibers without any evidence of damage could also be observed. The laser cuts induced close to the threshold exhibited only localized corneal tissue modifications. Moreover, some cavitation bubbles remain 36 h after the laser incisions that are much smaller than the ones imaged just after the surgery, a few tens versus a few hundreds of micrometers. The size variations can be explained by the cavitation bubbles resorption within the first hours after laser surgery.

Perforating femtosecond laser incisions (see Video 4) were investigated and we observe that the laser produces a regular incision of constant good quality across the depth of the cornea. A perturbation of the collagen structure as in lamellar incisions can be observed and irregular residual cavities remain present in the corneal tissue with dimensions up to several tens of micrometers. Obviously, although the incident pulse energy is kept constant, the laser beam broadening and attenuation due to the opacity of the tissue result in stronger disruption effects in the anterior part of the cornea than in the

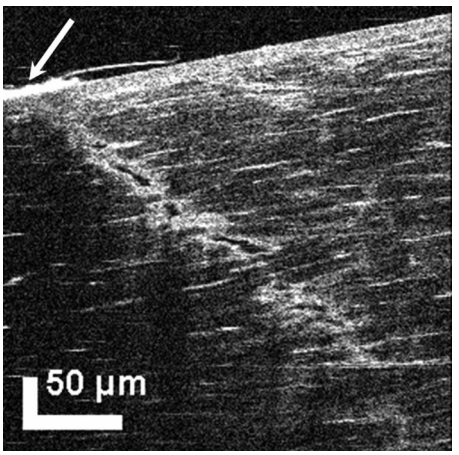

Video 4 Two-dimensional tomographic images along the axial direction where the perforating laser incisions have been realized; scale bar is 50 μm ($250\times190\times400$ μm^3 stack, with 0.5-μm axial steps). The laser incisions on the surface on the cornea (arrow) show a hyperreflective structure (QuickTime, 2.5 MB).
[URL: http://dx.doi.org/10.1117/1.3486544.4].

posterior region. At the surface of the vertical side cuts, OCT imaging seems to show a more reflective interface (arrow in Video 4) than on the other parts of the cornea surface. This could be due to the laser incisions in the upper layer of the cornea. This hyperreflective interface and the modification of the stroma structure with the presence of cavitation bubbles could induce the lack of signal from the deeper structures in this region observed in the lower left corner of the images. For OCT imaging, the cornea is illuminated from the anterior part (according to the vertical direction on the presented images) and the previous modifications of the structure could explain the shadow because the propagation of the light beam is modified and, hence, the penetration depth is smaller in this region.

4 Discussion and Perspectives

FF-OCT is particularly suited for imaging the fine structures of human cornea. The developed device reaches ultrahigh 3-D resolution imaging (respectively, 1 and 1.5 μm in the axial and transverse directions) and, hence, enables an imaging quality close to traditional histological sections observed with classical optical microscopes. Moreover, OCT presents the advantage of 3-D imaging, with virtual sectioning along chosen directions, on unstained samples and without any slicing. Indeed imaging of the entire thickness of the cornea at a micrometer scale could provides key information about the characteristics of this tissue[41] (thickness, hydration degree). This highlights the technique as a powerful tool for the study of pathologies on *ex vivo* human cornea. These requirements involve the precise anatomical and histological determination of each corneal layer, including the two thin posterior layers of the cornea, the endothelium and Descemet's membrane. With our FF-OCT setup, imaging of an edematous cornea showed the presence of lakes and the evolution of the structure by comparison with a nonedematous tissue. A further study of the development of edema in the cornea and of the swelling and deswelling processes that occur on donor corneas before corneal grafts could be of great interest. FF-OCT also appears as an interesting tool for a better characterization of the donor graft (stroma and endothelial cells). Then, this technique could be used in the Eye Banks for graft selection.

The main drawback of FF-OCT is that it requires relatively long acquisition times compared to FD-OCT. Nevertheless, it provides volumic imaging with a high and homogeneous 3-D spatial resolution. Although some studies[42–44] have shown *in vivo* imaging with FF-OCT, this configuration leads to a tradeoff between high-speed imaging and sensitivity of the device. Our system was specifically developed for *ex vivo* imaging. Hence, any sample movement during the acquisition time would blur the interference signal. Nevertheless, this choice was motivated by the aim of imaging with high resolution edematous tissues and laser incisions in quite deep regions of the corneal stroma for diagnostic studies. The implementation of polarizing elements could also give access to a better imaging of the laser incisions. By locally modifying the tissue structure, the laser incisions would be identified by specific polarimetric signatures that could be detected[35,45,46] by polarization-sensitive OCT. The cornea exhibits birefringence mainly due to collagen, and the laser surgery could induce a modification of these properties. These signatures could also be correlated with the influence of laser parameters.

As the corneal graft has grown to be the most frequently performed tissue transplant in the world, surgical improvements lead to a gradual change in procedures. Alternatives to standard penetrating keratoplasty (PK) were developed, such as anterior or posterior lamellar grafting procedures, for which only the pathological layer of the patient's cornea is replaced.[47,48] Laser-assisted processing is the most appropriate method to perform these manually complicated dissections. This requirement of deep and precise corneal surgery with high ablation accuracy combined with minimal damage to the healthy surrounding tissues is ideally obtained with ultrashort lasers such as femtosecond lasers. The advent of femtosecond lasers has sparked a great interest in the search for finer effects, better accuracy, control, and reliability of the surgical process. However, femtosecond laser corneal operations use fluence values much greater than the damage threshold of tissues, leading to nonoptimized resolution and interface quality, particularly in important areas in nonhealthy tissue.[49] Currently, the challenge is to optimize clinical operating conditions to cut as regularly as possible deep corneal tissues without damaging the surrounding zones. This implies working close to the damage or ablation threshold.[50] The imaging of laser incisions presented here reveals a change of the structure due to the disruption of the tissue and the presence of cavitation bubbles. Both aspects induce a refractive index modification that leads to a tomographic signal. FF-OCT appears as an interesting technique for characterization of laser effects into graft corneal tissue. Furthermore, as edematous and nonedematous corneas do not have the same optical properties, the laser disruption effects vary as a function of edema. It could then be interesting to obtain precise characteristics of the state of the corneal graft stroma and to adjust laser incisions settings to these parameters. Moreover, new sources, with wavelengths minimizing the scattering and the absorption phenomena across the tissue,[51] could be combined with high-resolution imaging methods to determine the ablation threshold in the stroma, to evaluate the profile and the quality

of the laser incisions, and to optimize the laser parameters for corneal tissue cutting.

5 Conclusion

We demonstrated that the use of micrometer-scale resolution FF-OCT enables large-scale imaging of all the layers of a human cornea with subcellular resolution. Large-scale micrometric resolved acquisitions are important, since they provide images of the entire corneal thickness. Longitudinal cross section corneal imaging could help to characterize pathologic tissues and to observe laser damage characteristics in the corneal volume. These findings are relevant for clinical applications, since they could give access to the development of a high-quality laser-cutting surgery process for ocular tissues. FF-OCT will offer unique opportunities for the development of new noninvasive tools for *ex vivo* corneal imaging. FF-OCT appears as a very effective approach for imaging the structure and corneal pathologies as well as laser incisions on *ex vivo* human cornea.

Acknowledgments

The authors acknowledge the French Blood Center of Marseille (France) and particularly Dr. Y. Nouaille de Gorce for providing samples of human graft cornea. We thank J. Moreau and D. Sacchet (Laboratoire Charles Fabry) and M. C. Schanne-Klein and E. Beaurepaire (Laboratoire d'Optique et Biosciences) for fruitful discussions and O. Casadessus for experimental help. This research was supported by the PACA region.

References

1. M. A. Lemp, P. N. Dilly, and A. Boyde, "Tandem-scanning microscopy of the full-thickness of the cornea," *Cornea* **4**, 205–209 (1985).
2. M. Böhnke and B. R. Masters, "Confocal microscopy of the cornea," *Prog. Retin Eye Res.* **18**(5), 553–628 (1999).
3. B. Sonigo, V. Iordanidou, D. Chong-Sit, F. Auclin, J. M. Ancel, A. Labbé, and C. Baudouin, "*In vivo* corneal confocal microscopy comparison of intralase femtosecond laser and mechanical microkeratome for laser *in situ* keratomileusis," *Invest. Ophthalmol. Visual Sci.* **47**(7), 2803–2811 (2006).
4. J. C. Erie, J. W. McLaren, and S. V. Patel, "Confocal microscopy in ophthalmology," *Am. J. Ophthalmol.* **148**, 639–646 (2009).
5. D. W. Piston, B. R. Masters, and W. W. Webb, "Three-dimensionally resolved NAD(P)H cellular metabolic redox imaging of the *in situ* cornea with two-photon excitation laser scanning microscopy," *J. Microsc.* **178**, 20–27 (1995).
6. M. Han, G. Giese, and J. F. Bille, "Second harmonic generation imaging of collagen fibrils in cornea and sclera," *Opt. Express* **13**(15), 5791–5797 (2005).
7. J. G. Lyubovitsky, J. A. Spencer, T. B. Krasieva, B. Andersen, and B. J. Tromberg, "Imaging corneal pathology in a transgenic mouse model using nonlinear microscopy," *J. Biomed. Opt.* **11**(1), 014013 (2006).
8. B. G. Wang, K. Koenig, I. Rieman, R. Krieg, and K. J. Halbhuber, "Intraocular multiphoton microscopy with subcellular spatial resolution by infrared femtosecond lasers," *Histochem. Cell Biol.* **126**, 507–515 (2006).
9. N. Morishige, A. J. Wahlert, M. C. Kenney, D. J. Brown, K. Kawamoto, T. Chikama, T. Nishida, and J. V. Jester, "Second-harmonic imging microscopy of normal human and keratoconus cornea," *Invest. Ophthalmol. Visual Sci.* **48**(3), 1087–1093 (2007).
10. F. Aptel, N. Olivier, A. Deniset-Besseau, J. M. Legeais, K. Plamann, M. C. Schanne-Klein, and E. Beaurepaire, "Multimodal nonlinear imaging of the human cornea," *Invest. Ophthalmol. Visual Sci.* **51**, 2459–2465 (2010).
11. D. Huang, E. A. Swanson, C. P. Lin, J. S. Schuman, W. G. Stinson, W. Chang, M. R. Hee, T. Flotte, K. Gregory, C. A. Puliafito, and J. G. Fujimoto, "Optical coherence tomography," *Science* **254**, 1178–1181 (1991).
12. A. F. Fercher, W. Drexler, C. K. Hitzenberger, and T. Lasser, "Optical coherence tomography—principles and application," *Rep. Prog. Phys.* **66**(2), 239–303 (2003).
13. M. Wojtkowski, R. Leitgeb, A. Kowalczyk, T. Bajraszewski, and A. F. Fercher, "*In vivo* human retinal imaging by Fourier domain optical coherence tomography," *J. Biomed. Opt.* **7**(3), 457–463 (2002).
14. W. Drexler and J. G. Fujimoto, "State-of-the-art retinal optical coherence tomography," *Prog. Retin Eye Res.* **27**, 45–88 (2008).
15. J. A. Izatt, M. R. Hee, E. A. Swanson, C. P. Lin, D. Huang, J. S. Schuman, C. A. Puliafito, and J. G. Fujimoto, "Micrometer-scale resolution imaging of the anterior eye *in vivo* with optical coherence tomography," *Arch. Ophthalmol.* **112**, 1584–1589 (1994).
16. M. Gora, K. Karnowski, M. Szkulmowski, B. J. Kaluzny, R. Huber, A. Kowalczyk, and M. Wojtkowski, *Opt. Express* **17**(17), 14880–14894 (2009).
17. E. Beaurepaire, A. C. Boccara, M. Lebec, L. Blanchot, and H. Saint-Jalmes, "Full-field optical coherence microscopy," *Opt. Lett.* **23**(4), 244–246 (1998).
18. A. Dubois, L. Vabre, C. Boccara, and E. Beaurepaire, "High-resolution full-field optical coherence tomography with a Linnik microscope," *Appl. Opt.* **41**(4), 805–812 (2002).
19. A. Dubois, K. Grieve, G. Moneron, R. Lecaque, L. Vabre, and A.-C. Boccara, "Ultrahigh-resolution full-field optical coherence tomography," *Appl. Opt.* **43**(14), 2874–2883 (2004).
20. K. Grieve, M. Paques, A. Dubois, J. Sahel, C. Boccara, and J. F. Le Gargasson, "Ocular tissue imaging using ultrahigh-resolution full-field optical coherence tomography," *Invest. Ophthalmol. Visual Sci.* **45**(11), 4126–4131 (2004).
21. M. Akiba, N. Maeda, K. Yumikake, T. Soma, K. Nishida, Y. Tano, and K. P. Chan, "Ultrahigh-resolution imaging of human donor cornea using full-field optical coherence tomography," *J. Biomed. Opt.* **12**(4), 041202 (2007).
22. M. Han, G. Giese, L. Zickler, H. Sun, and J. F. Bille, "Mini-invasive corneal surgery and imaging with femtosecond lasers," *Opt. Express* **12**(18), 4275–4281 (2004).
23. M. Niemz, *Laser-Tissue Interactions—Fundamentals and Applications*, 3rd ed., Springer, Heidelberg (2003).
24. J. Bille, C. Harner, and F. H. Loesel, *New Frontiers in Vision and Aberration-Free Refractive Surgery*, Springer, Heidelberg (2002).
25. K. Koenig, B. Wang, I. Riemann, and J. Kobow, "Cornea surgery with nanojoule femtosecond laser pulses," *Proc. SPIE* **5688**, 288–293 (2005).
26. H. K. Soong and J. B. Malta, "Femtosecond lasers in ophthalmology," *Am. J. Ophthalmol.* **147**(2), 189–197 (2009).
27. T. Juhasz, F. Loesel, R. Kurtz, C. Horvath, J. F. Bille, and G. Mourou, "Corneal refractive surgery with femtoseconds lasers," *IEEE J. Sel. Top. Quantum Electron.* **5**(4), 902–910 (1999).
28. L. Hoffart, H. Proust, F. Matonti, B. Ridings, and J. Conrath, "Short-term results of penetrating keratoplasty performed with the Femtec femtosecond laser," *Am. J. Ophthalmol.* **146**(1), 50–55 (2008).
29. M. A. Terry, P. J. Ousley, and B. Will, "A practical femtosecond laser procedure for DLEK endothelial transplantation: cadaver eye histology and topography," *Cornea* **24**(4), 453–459 (2005).
30. B. Seitz, H. Brunner, A. Viestenz, C. Hofmann-Rummelt, U. Schlotzer-Schrehardt, G. O. Naumann, and A. Langenbucher, "Inverse mushroom-shaped nonmechanical penetrating keratoplasty using a femtosecond laser," *Am. J. Ophthalmol.* **139**(5), 941–944 (2005).
31. T. S. Ignacio, T. B. Nguyen, R. S. Chuck, R. M. Kurtz, and M. A. Sarayba, "Top hat wound configuration for penetrating keratoplasty using the femtosecond laser: a laboratory model," *Cornea* **25**(3), 336–340 (2006).
32. A. Vogel, J. Noack, G. Huttman, and G. Paltauf, "Mechanisms of femtosecond laser nanosurgery of cells and tissues," *Appl. Phys. B* **81**(8), 1015–1047 (2005).
33. A. Heisterkamp, T. Mamom, W. Drommer, W. Ertner, and H. Lubatschowski, "Photodisruption with ultrashort laser pulses for intrastromal refractive surgery," *Laser Phys.* **13**(5), 743–748 (2003).
34. V. Nuzzo, K. Plamann, M. Savoldelli, F. Aptel, B. Reynier, F. Pailloux, T. Cabioc'h, O. Albert, and J. M. Legeais, "Deposit of glass fragments during femtosecond laser penetrating keratoplasty," *Graefe's Arch. Clin. Exp. Ophthalmol.* **247**(1), 107–113 (2009).
35. Y. Yasuno, M. Yamanari, K. Kawana, T. Oshika, and M. Miura, "In-

vestigation of post-glaucoma-surgery by three-dimensional and polarization sensitive anterior eye segment optical coherence tomography," *Opt. Express* **17**(5), 3980–3995 (2009).
36. J. S. Brown, D. Wang, X. Li, F. Baluyot, B. Iliakis, T. D. Lindquist, R. Shirakawa, T. T. Shen, and X. Li, "*In situ* ultrahigh-resolution optical coherence tomography characterization of eye bank corneal tissue processed for lamellar keratoplasty," *Cornea* **27**(7), 802–810 (2008).
37. A. Dubois, G. Moneron, K. Grieve, and A. C. Boccara, "Three-dimensional cellular-level imaging using full-field optical coherence tomography," *Phys. Med. Biol.* **49**, 1227–1234 (2004).
38. A. Dubois, G. Moneron, and C. Boccara, "Thermal-light full-field optical coherence tomography in the 1.2 μm wavelength region," *Opt. Commun.* **266**, 738–743 (2006).
39. G. B. Benedek, "Theory of transparency of the eye," *Appl. Opt.* **10**(3), 459–473 (1971).
40. R. A. Farrell, R. L. McCally, and P. E. R. Tatham, "Wave-length dependencies of light scattering in normal and cold swollen rabbit corneas and their structural implications," *J. Physiol.* **233**, 589–612 (1973).
41. A. C. M. Wong, C. C. Wong, N. S. Y. Yuen, and S. P. Hui, "Correlational study of central corneal thickness measurements on Hong Kong Chinese using optical coherence tomography, Orbscan and ultrasoundpachymetry," *Eye* **16**(6), 715–721 (2002).
42. K. Grieve, A. Dubois, M. Simonutti, M. Paques, J. Sahel, J. F. Le Gargasson, and C. Boccara, "*In vivo* anterior segment imaging in the rat eye with high speed white light full-field optical coherence tomography," *Opt. Express* **13**(16), 6286–6295 (2005).
43. G. Moneron, C. Boccara, and A. Dubois, "Stroboscopic ultrahigh-resolution full-field optical coherence tomography," *Opt. Lett.* **30**(11), 1351–1353 (2005).
44. M. Akiba and K. P. Chan, "*In vivo* video-rate cellular-level full-field optical coherence tomography," *J. Biomed. Opt.* **12**(6), 064024 (2007).
45. G. Moneron, A.-C. Boccara, and A. Dubois, "Polarization-sensitive full-field optical coherence tomography," *Opt. Lett.* **32**(14), 2058–2060 (2007).
46. E. Götzinger, M. Pircher, M. Sticker, A. F. Fercher, and C. K. Hitzenbzerger, "Measurement and imaging of birefringent properties of the human cornea with phase-resolved, polarization-sensitive optical coherence tomography," *J. Biomed. Opt.* **9**(1), 94–102 (2004).
47. M. O. Price and F. W. Price, "Descemet's stripping with endothelial keratoplasty: comparative outcomes with microkeratome-dissected and manually dissected donor tissue," *Ophthalmology* **113**(11), 1936–1942 (2006).
48. G. R. Melles, F. Lander, B. T. van Dooren, E. Pels, and W. H. Beekhuis "Preliminary clinical results of posterior lamellar keratoplasty through a sclerocorneal pocket incision," *Ophthalmology* **107**(10), 1850–1856 (2000).
49. E. M. Perlman, "An analysis and interpretation of refractive errors after penetrating keratoplasty," *Ophthalmology* **88**, 39–45 (1981).
50. P. S. Binder, M. Sarayba, T. Ignacio, T. Juhasz, and R. Kurtz, "Characterization of submicrojoule femtosecond laser corneal tissue dissection," *J. Cataract Refractive Surg.* **34**(1), 146–152 (2008).
51. F. Morin, F. Druon, M. Hanna, and P. Georges, "Microjoule femtosecond fiber laser at 1.6 μm for corneal surgery applications," *Opt. Lett.* **34**(13), 1991–1993 (2009).